ACS APPLIED MATERIALS & INTERFACES

www.acsami.org

Research Article

Optically Modulated HfS_2-Based Synapses for Artificial Vision Systems

Hao Xiong, Liping Xu, Caifang Gao, Qing Zhang, Menghan Deng, Qiangfei Wang, Jinzhong Zhang,* Dirk Fuchs, Wenwu Li, Anyang Cui, Liyan Shang, Kai Jiang, Zhigao Hu,* and Junhao Chu

Cite This: *ACS Appl. Mater. Interfaces* 2021, 13, 50132−50140

Read Online

ACCESS | Metrics & More | Article Recommendations | Supporting Information

ABSTRACT: The simulation of human brain neurons by synaptic devices could be an effective strategy to break through the notorious "von Neumann Bottleneck" and "Memory Wall". Herein, opto-electronic synapses based on layered hafnium disulfide (HfS_2) transistors have been investigated. The basic functions of biological synapses are realized and optimized by modifying pulsed light conditions. Furthermore, 2 × 2 pixel imaging chips have also been developed. Two-pixel visual information is illuminated on diagonal pixels of the imaging array by applying light pulses (λ = 405 nm) with different pulse frequencies, mimicking short-term memory and long-term memory characteristics of the human vision system. In addition, an optically/electrically driven neuromorphic computation is demonstrated by machine learning to classify hand-written numbers with an accuracy of about 88.5%. This work will be an important step toward an artificial neural network comprising neuromorphic vision sensing and training functions.

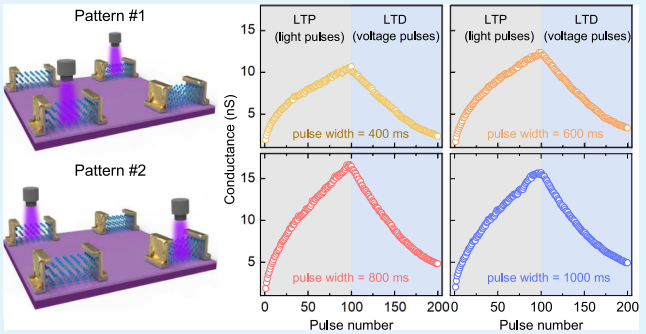

KEYWORDS: *two-dimensional layered materials, hafnium disulfide, opto-electronic synapses, artificial vision systems, pattern recognition*

1. INTRODUCTION

In neurobiology, exploring and mimicking the biological perception mechanism concerning human brain neurons are an important research area.[1,2] Complicated information processing strategies are very efficient since calculation and memory storage occur in one action by adjusting the connection strength.[3] Therefore, the concept of "brain-like engineering" is proposed based on the operation mechanism of neural networks, which is different from that of traditional computers designed by the von Neumann architecture.[4,5] Artificial neural networks (ANNs) can emulate human brain functions (learning, multiobject detection, classification, recognition, etc.) by low-power consumption and high-efficiency parallel multitasking at hardware levels, which could overcome the notorious "von Neumann Bottleneck" and "Memory Wall".[6−9] The human brain consists of billions of neuronal cells connected by synapses. Thus, synaptic plasticity has been a focus of attention as the crucial substrate of synaptic memory and learning. Information can be processed and stored at the same time by adjusting the synapse weight.[10] Therefore, it is crucial to emulate different synaptic functions based on the concept of bioelectronics to develop neuromorphic engineering, especially simulating the human visual system.[11,12]

It is well known that the human visual system consists of three basic parts: retina, optic nerve, and visual cortex.[12,13] The cone cells and rod cells on the retina can sense light signals and convert them into electrical signals. The electrical signals are transmitted to ganglion cells through bipolar cells and horizontal cells, finally forming optical fibers which can transmit signals to the visual center in the brain. Synaptic devices act as cone cells and rod cells in the artificial retina system. More opto-electronic synaptic transistors will be integrated in ANNs with the development of optical interconnection technology. Optical information has the advantages of low transmission loss and strong anti-interference ability.[14] Therefore, research on the function of a visual system is mainly focused on the opto-electronic synaptic devices.[8,11,12,15] Recently, two-dimensional (2D) layered transition-metal dichalcogenides exhibit excellent electrical and optical properties due to the unique internal and interfacial structure,[16−19] making them channels of transistors for artificial synaptic devices.[20−24] For the case of hafnium disulfide (HfS_2), it has a super high theoretical acoustic-phonon-limited mobility (1800−3500 $cm^2\ V^{-1}\ s^{-1}$) and a wide photo-electric response range (1−2 eV) with a band gap of about 1.2 eV.[24,25] In particular, the photo-

Received: August 2, 2021
Accepted: October 4, 2021
Published: October 18, 2021

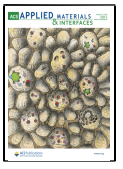

https://doi.org/10.1021/acsami.1c14332
ACS Appl. Mater. Interfaces 2021, 13, 50132−50140

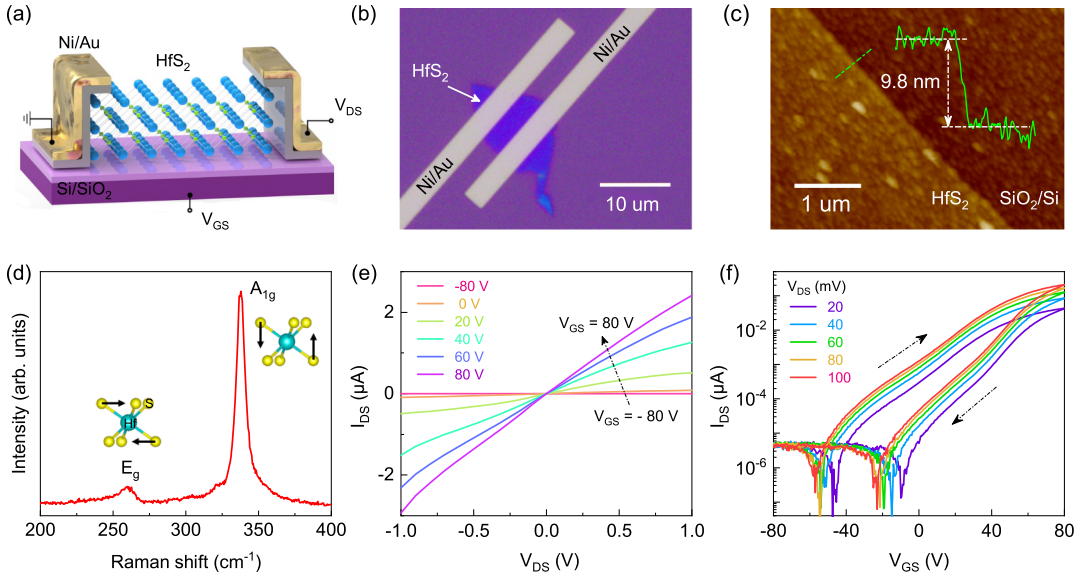

Figure 1. (a) Schematic illustration of a HfS_2-based field effect transistor. (b) Optical image of the HfS_2-based synaptic transistor. (c) AFM image of the HfS_2 sheet on the SiO_2/Si substrate. Inset: the line profile of a HfS_2 sheet. (d) Raman spectrum of the HfS_2 sheet used in the device. The two peaks located at about 260 and 338 cm^{-1} are assigned to the first-order Raman-active modes E_g and A_{1g}, respectively. (e) Output and (f) transfer characteristic curves of the transistor in a dark environment at room temperature.

responsivity of HfS_2 can reach 890 A/W and photogain over 2300 under a back-gate voltage of 80 V.[26] Besides, HfS_2 contains Hf elements, and it is easy to integrate with the high-k material HfO_2.[27] The ultra-high responsiveness and compatibility with silicon lay a good foundation for the use of optical synapses.

Herein, we have investigated the electronic and photoelectric properties of HfS_2-based synaptic transistors and arrays in detail. The synaptic plasticity behavior including short-term plasticity (STP), paired-pulse facilitation (PPF), long-term potentiation (LTP), long-term depression (LTD), and so forth have been well mimicked by our HfS_2-based synapses. Furthermore, the 2 × 2 pixel imaging chips are fabricated for the integration of a synaptic device into an artificial vision system. In addition, the continuous increase/decrease of synapse weight of LTP/LTD is emulated by applying light and voltage pulses, respectively. The conductance states of LTP/LTD show a stable and linear increase/decrease. Finally, a 784 × 150 × 10 ANN is conducted for pattern recognition with an accuracy of 88.5%. These results indicate that optically modulated HfS_2-based synapses can be well applied to artificial vision systems.

2. MATERIALS AND METHODS

2.1. HfS_2-Based Device Fabrication. Few-layer HfS_2 flakes were mechanically exfoliated from a bulk HfS_2 single crystal and then dry-transferred to 280 nm thick SiO_2/Si substrates with predefined markers for electron beam lithography. A two-layer (copolymer/950 K) polymethyl methacrylate resist system was adopted to realize an ideal shape of Ni/Au (2/60 nm) electrodes without side walls, which were evaporated via a thermal evaporator. For the fabrication of a synapse array architecture, the spacing between two HfS_2-based devices is about 3 mm.

2.2. Characterization. The morphology and thickness of as-transferred HfS_2 flakes were measured using an optical microscope and an atomic force microscope (Dimension Icon, Bruker). A confocal micro-Raman spectrometer (Jobin-Yvon LabRAM HR Evolution, HORIBA) with a 532 nm excitation laser line was used to detect the lattice vibrations of 2D layered semiconductor HfS_2.

2.3. Synaptic Plasticity of the HfS_2-Based Transistors. A Keithley 4200-SCS semiconductor parameter analyzer was used for electronic and photo-electric measurements of HfS_2-based synaptic transistors. All measurements are performed under vacuum conditions and dark conditions with exposure to the target light sources only. For the photo-electric measurements, a commercial light-emitting diode with an illumination wavelength of 405 nm (Thorlabs, Inc.) was employed. Light pulse with tunable power intensity, pulse width, and frequency were controlled using a laser diode/temperature controller (ITC4001, Thorlabs, Inc.). The pulsed gate voltage was generated by a semiconductor pulse generator unit module.

2.4. Neural Network Simulation. A multiple-layer perceptron neural network with an interval hidden feature vector is conducted on the basis of the CrossSim (Pytorch) platform.[28] The network consists of an input layer (784 neurons), a hidden layer (150 neurons), and an output layer (10 neurons). The neural network simulations are carried out on a image version (28 × 28 pixels) of hand-written digits from the Modified National Institute of Standards and Technology (MNIST) data set. Therefore, the network size is 784 × 150 × 10. After training with randomly selected 8000 images per epoch from 60 000 images of the training data set, the recognition accuracy of 10 digits is estimated by using 10 000 images from a separate testing data set.

3. RESULTS AND DISCUSSION

3.1. Structure and Electrical Properties of HfS_2-Based Transistors. Figure 1a shows a schematic illustration of a HfS_2-based field effect transistor. Details for the fabrication of HfS_2-based devices can be founded in Section 2.1. As shown in Figures 1b and S1a (Supporting Information), the HfS_2-based devices are fabricated in a transistor configuration. The concentration of the carriers in the channel can be modulated by applying various gate voltages.[22,29] In Figure 1c, the AFM image and the corresponding line profile clearly express the HfS_2 thickness of about 9.8 nm (i.e., ~16 layers). Note that the HfS_2 flake with a finite thickness of 7−12 nm can bring a high performance of the HfS_2-based transistor. Figure 1d illustrates the Raman spectrum of a HfS_2 sheet, which is similar to that of HfS_2 single crystals (cf. Figure S1b, Supporting Information). According to the D_{3d}^3 ($P\bar{3}m1$) space-group symmetry of HfS_2,

https://doi.org/10.1021/acsami.1c14332
ACS Appl. Mater. Interfaces 2021, 13, 50132−50140

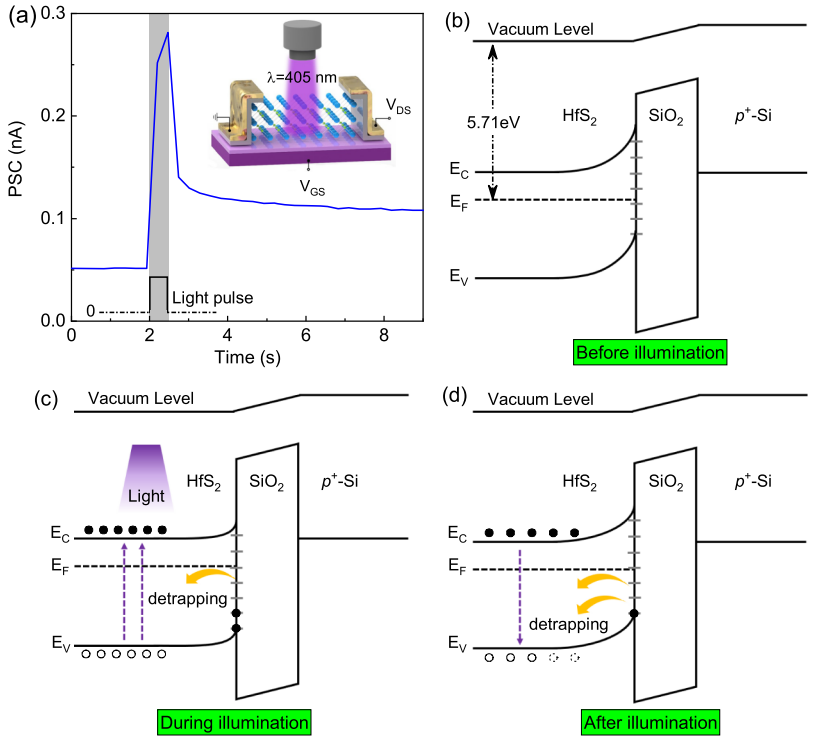

Figure 2. (a) Typical behavior of the PSC under a single light spike stimulation. The inset shows the schematic diagram of an artificial synaptic opto-electronic transistor under light illumination (λ = 405 nm). Light stimulation (gate electrodes) connects with pre-synaptic neurons (writing) and drain/source electrodes connect with post-synaptic neurons (reading). Energy band diagrams of the $HfS_2/SiO_2/p^+$-Si architecture for the cases (b) before, (c) during, and (d) after illumination.

the two peaks near 260 and 338 cm^{-1} are assigned to the first-order Raman-active modes E_g and A_{1g}, respectively. Theoretically, the two Raman-active modes E_g and A_{1g}, predicted at the Γ point belong to the in- and out-plane modes, respectively.[26,30] The corresponding lattice vibrations are sketched in Figure 1d. The results suggest that the as-transferred HfS_2 sheets are of high quality, which could exhibit better electronic and photo-electric behavior for artificial vision systems.

The basic electrical performance of HfS_2-based transistors is measured in a high-vacuum environment ($\sim 10^{-6}$ Torr). The devices in this work are back-gated field effect transistors fabricated on p^+-Si/SiO_2 substrates. Therefore, the source-drain current mostly occurs near the interface at HfS_2/SiO_2. The output characteristics show that the drain-source current (I_{DS}) changes linearly as a function of the drain-source voltage (V_{DS}) under various gate voltages (V_{GS}) from −80 to +80 V, as depicted in Figure 1e. It indicates that a good Ohmic contact is formed between the channel and electrodes. Figure 1f shows the transfer characteristic curves as a function of V_{GS} measured by applying various V_{DS} from 20 to 100 mV with a step of 20 mV, suggesting an *n*-type feature of the HfS_2-based transistor. The hysteresis between the forward and backward curves is mainly due to the charge trapping at the interface between HfS_2 and SiO_2.[31] To explore the origin of the hysteresis for devices with a p^+-$Si/SiO_2/HfS_2$ structure, a layer of *h*-BN was inserted between HfS_2 and SiO_2. As shown in Figure S2a (Supporting Information), the hysteresis of the transfer characteristic curve for devices with the p^+-Si/SiO_2/*h*-BN/HfS_2 structure can be negligible. Therefore, the HfS_2/SiO_2 interface dominates the memory behavior. Moreover, a nonlinear double-slope transfer curve could originate from the surface adsorbate, mobile ions, gate voltage-induced stress, or interface traps.[17,32] The electron mobility of about 1−3 cm^2 V^{-1} s^{-1} and on/off current ratio ($\sim 10^5$) is obtained from the representative transfer curves. Furthermore, the transfer characteristics are investigated under dark and light irradiation conditions (cf. Figure S2b, Supporting Information). The I_{DS} in the transfer curves becomes larger as the light power density increases, which means that more photo-generated carriers are generated with increasing light power density. The device performance is pivotal to the consistency of device operations and the simulation of synaptic behavior. Therefore, we provided the statistical distribution of the performance of 20 fabricated devices in transfer characteristic curves, on/off ratio, mobility, and threshold voltages (V_{th}) as shown in Figure S3 (Supporting Information), which indicates our devices have a good reproducibility.

3.2. Synaptic Plasticity of the HfS_2-Based Transistors.

In neurobiology of vision, photo-receptor neurons on the retina are the basis for the human visual system to perceive or receive external light signals.[33] In order to simulate the opto-synaptic dynamics, a 405 nm laser is irradiated vertically on the HfS_2-based synaptic transistors, as illustrated in the inset of Figure 2a. Here, the drain electrode is defined as a post-synaptic terminal, which connects to post-synaptic neurons. Their connection strength (synaptic weight) can be adjusted by an external stimulus, which is mapped to synaptic transistors.[34] Zhang et al. reported that the work function and band gap of HfS_2 are 5.71 and 1.13 eV, respectively.[35] Figure 2a shows a typical behavior of post-synaptic current (PSC) in a spike stimulation, which includes three stages: before, during, and after illumination. Before illumination, the energy band of the semiconductor surface is bent upward when HfS_2 is in contact with the p^+-Si/SiO_2 substrate due to the

https://doi.org/10.1021/acsami.1c14332
ACS Appl. Mater. Interfaces 2021, 13, 50132−50140

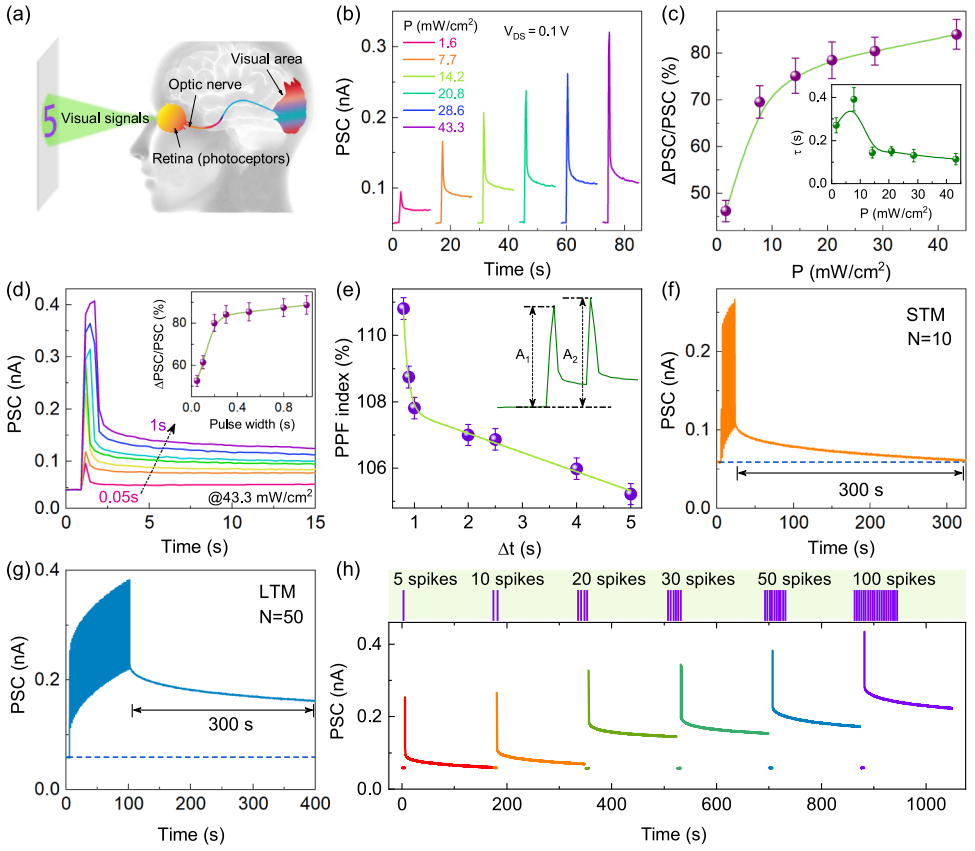

Figure 3. (a) Schematic diagram of the human optic nerve system. (b) PSC stimulated by a single light pulse with different power densities from 1.6 to 43.3 mW/cm^2 at a fixed pulse width (0.5 s). (c) Corresponding weight change (ΔPSC/PSC) as a function of light power density. Inset: The extracted retention time τ as a function of light power intensity based on the Kohlrausch law. (d) PSC stimulated by a series of light pulses with the same power density (43.3 mW/cm^2) and different light pulse widths from 50 ms to 1 s. The inset is the corresponding weight change as a function of the light pulse width. (e) PPF index and the best-fitted curve as a function of the paired pre-synaptic spike interval Δt. Inset: PSC amplitudes (A_1 and A_2) caused by a pair of light pulses. (f) STM and (g) LTM triggered by laser pulses (power density: 43.3 mW/cm^2 and pulse width: 0.5 s) with different pulse numbers. (h) PSC curves after various numbers of light pulses (pulse width: 0.5 s and pulse period: 2 s). Note that all the PSC (I_{DS}) measurements are carried out by applying a V_{DS} of 0.1 V.

surface defects of SiO_2 (Si−O dangling bonds and movable positive charges) as shown in Figure 2b. During illumination, a large number of photo-generated electrons and holes will rapidly generate in the channel, and the upward bending trend of the energy band will be greatly reduced (cf. Figure 2c). At this time, the channel current will increase rapidly. After stimulation, as shown in Figure 2d, the photo-generated electrons quickly recombine with holes, and the current drops. However, the current cannot drop to the initial state before illumination in a short time since a part of trapped electrons can be released by the interface traps. The current drop in the channel is alleviated. The upward curvature of the energy band of the semiconductor surface increases. Therefore, the interface defects dominate the channel current and memory behavior in this way.

Figure 3a shows the schematic diagram of the human optic nerve system. The visual system of human eyes can be considered as a combination of three parts in sequence,[33] the retina located inside the back wall of human eyes, the lateral geniculate located in the thalamus, and the visual cortex of the brain. In this work, the HfS_2-based devices were employed as optic-neural synapses that execute the optical-seeing functions. For the case of synaptic devices, the conductance states in the channel are modulated by applying a light pulse to mimic the synaptic weight of biological synapses. In the HfS_2-based synapses, the layered HfS_2 has ultrahigh responsivity, photogain, and fast response time, which provide a foundation for finely controlling channel current by a low-energy light pulse. Since synaptic plasticity is very susceptible to environmental and historical activities, the artificial synaptic plasticity of HfS_2-based synaptic devices has been explored systematically by applying light pulses with various parameters such as power density, pulse width, pulse number, and frequency. Figure 3b plots the PSC measured by applying a fixed V_{DS} (0.1 V) and various power densities (P) of a single light pulse (wavelength: 405 nm and pulse width: 0.5 s). The PSC increases with the increasing power density of the light pulse due to the generation of photo-carriers in HfS_2. Fortunately, a similar phenomenon is observed in biological excitatory synapses.[36] It indicates that our synaptic devices can simulate biological synaptic functions well, which can be used in artificial vision systems. Note that the PSC does not decay back to the resting current value, which indicates memory behavior.[37] Furthermore, the decay of the PSC was simulated by a parameterized Kohlrausch law $y = A_0 + A_1 \times \exp[-(t/\tau)^{\beta}]$.[38] For the case of laser power density of 43.3 mW/cm^2, the extracted stretch index (β) is 0.354 ± 0.007 and the retention time (τ) is about 128 ± 8 ms, which means that the feature time of the carrier migration is about 128 ms, as shown in Figure S3 and the inset of Figure 3c. The corresponding synaptic weight change (W)

https://doi.org/10.1021/acsami.1c14332
ACS Appl. Mater. Interfaces 2021, 13, 50132−50140

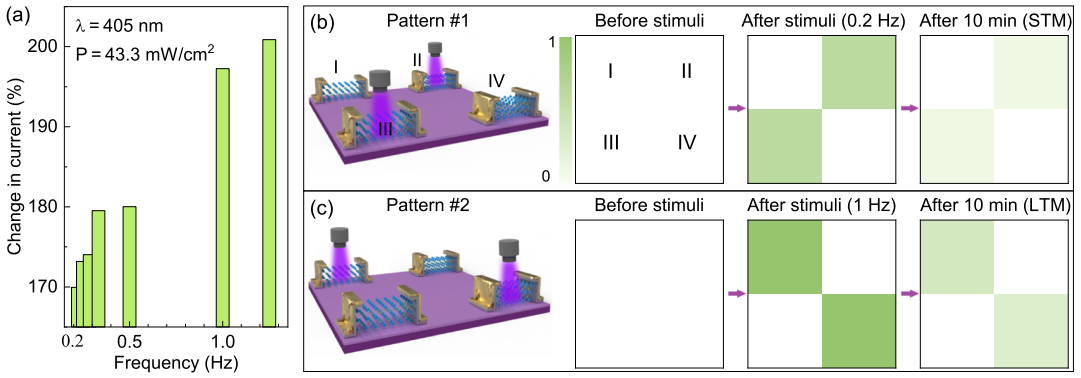

Figure 4. Imaging 2 × 2 array of information perception and memory based on HfS_2 synaptic devices. (a) Change in photocurrent of a synaptic transistor (single pixel) as a function of an illumination pulse frequency of a 405 nm laser with a power density of 43.3 mW/cm^2 and a pulse width of 500 ms. (b) Pattern #1 encoded by light pulses with a frequency of 0.2 Hz. The 2 × 2 pixel array demonstrates STM. (c) Encoding of Pattern #2 on the imaging array by light pulses with a frequency of 1 Hz, demonstrating LTM.

under various power densities of light pulses is plotted in Figure 3c. Here, $W = \Delta PSC/PSC=(A - A_0)/A \times 100\%$, where A and A_0 are the amplitudes of the PSC after a light simulation and initial level before light simulation, respectively. A higher optical power density provides high cumulative excitation energy, which results in the generation of higher photo-generated charge carriers in HfS_2 and weight changes. In addition, the spike-duration-dependent PSC shows that the excitatory response increases with increasing pulse width from 50 ms to 1 s (cf. Figure 3d). Note that the corresponding weight change has a rapid increase at about 0.3 s and then reaches a saturation point, which is similar to that in biological neurons.[39] In addition, the pulse-width-dependent PSC decay is evaluated based on the Kohlrausch law (cf. Figure S4). Note that the synaptic plasticity is well consistent with the synaptic behavior of human vision systems.

PPF is an important factor of STP, which manifests in the enhanced synaptic response caused by two consecutive stimuli in biological synapses.[40] Moreover, PPF is related to complex tasks performed by neurons, playing an important role in the process of decoding time information and audiovisual signals.[10] It appears that the PSC change caused by the second light stimulus is greater than that caused by the first light pulse. The PPF index of the HfS_2 synapse can be defined by the following formula:[11,41] PPF = $A_2/A_1 \times 100\%$, where A_1 and A_2 are the amplitudes of the first and second PSCs, respectively (cf. Figure 3e). The synaptic devices successfully simulate the PPF behavior of biological synapses and demonstrate the trend of the PPF index as a function of pulse interval (Δt) between two consecutive light stimuli. The PPF index decreases gradually from 111 to 105% with increasing Δt from 0.8 to 5 s. Note that the value of the PPF index is slightly smaller compared to other reported PPF indexes, which may be from the excellent photoelectric response performance of HfS_2 or a small laser power density.[24] In addition, the behavior can be simulated well by a parameterized double-exponential function:[11,24] The PPF index = $a_0 + a_1 \times \exp(-\Delta t/\tau_1) + a_2 \times \exp(-\Delta t/\tau_2)$ with two characteristic timescales $\tau_1 = 822 \pm 17$ ms and $\tau_2 = 11.1 \pm 1.3$ s, which are comparable to those measured in biological synapses.[42] Therefore, a narrow pulse width of 500 ms (less than τ_1) is applied in the following measurements for investigating the LTP behavior. In Figure 3f,g, light pulses with a fixed pulse width (0.5 s), pulse interval (0.5 s), and power density (43.3 mW/cm^2) are used to mimic the short-term memory (STM) and long-term memory (LTM) behaviors of the artificial synapses by changing the pulse number. Figure 3f shows that the STM behavior of the synapse device has been achieved by irradiating a series of light pulses (pulse number $N = 10$). The PSC decays and returns to the initial state in a short period of time. On the other hand, light pulses with the same intensity/width ($N = 50$) are applied, which induces an LTM behavior since the PSC decays slowly and there is a longer time of relaxation (cf. Figure 3g). The above results indicate that the transformation between STM and LTM in the HfS_2 synaptic devices can be realized by modulating the light pulse number. In order to further mimic the STM and LTM behaviors of artificial synapses, the light spikes with different pulse numbers ($N = 5$, 10, 20, 30, 50, and 100) are applied to stimulate the artificial synapses, as shown in Figure 3h. As the pulse number increases, the PSC increases. The behavior is similar to that of brain functions of learning, remembering, and forgetting.[43] As the number of learning increases, the memory is enhanced and harder to forget. The STM and LTM behaviors of synaptic devices are consistent with those of human visual synapses caused by light stimulation.

The spike rate is another important factor for assessing the plasticity of neuron synapses. The related learning behavior can be explained by the BCM (Bienenstock, Cooper, and Munro) theory.[44,45] In this work, the spike-rate-dependent plasticity of the HfS_2-based synapses has been investigated, as shown in Figure 4a. The change in current is derived by the relationship: $(A_{20} - A_1)/A_1 \times 100\%$. Here, A_{20} and A_1 are the PSC amplitudes of the 20th and first spikes, respectively.[8] At the low-frequency region below 0.5 Hz, it is much lower than that at a high frequency above 1.0 Hz. In a further step, 2 × 2 pixel imaging chips are fabricated using HfS_2-based transistors, which provide more possibilities for the integration of artificial synaptic devices into an artificial vision system. Note that the channel thickness of the four HfS_2-based devices is uniform in the range of 7−12 nm with a high performance. The light pulses with two typical spike rates are illuminated on the diagonal of the pixel array (cf. Figures 4b,c). It exhibits two illumination patterns (#1 and #2) stimulated by 30 continuous light pulses with the frequencies of 0.2 and 1 Hz, respectively. The PSC changes of the diagonal devices in the pixel array before stimulation (in the dark), soon after stimulation(<0.5 s), and 10 min after stimulation were measured to assess the memory/learning retention. For comparison, the PSCs of the four devices are normalized. It means that "0" corresponds to

https://doi.org/10.1021/acsami.1c14332
ACS Appl. Mater. Interfaces 2021, 13, 50132−50140

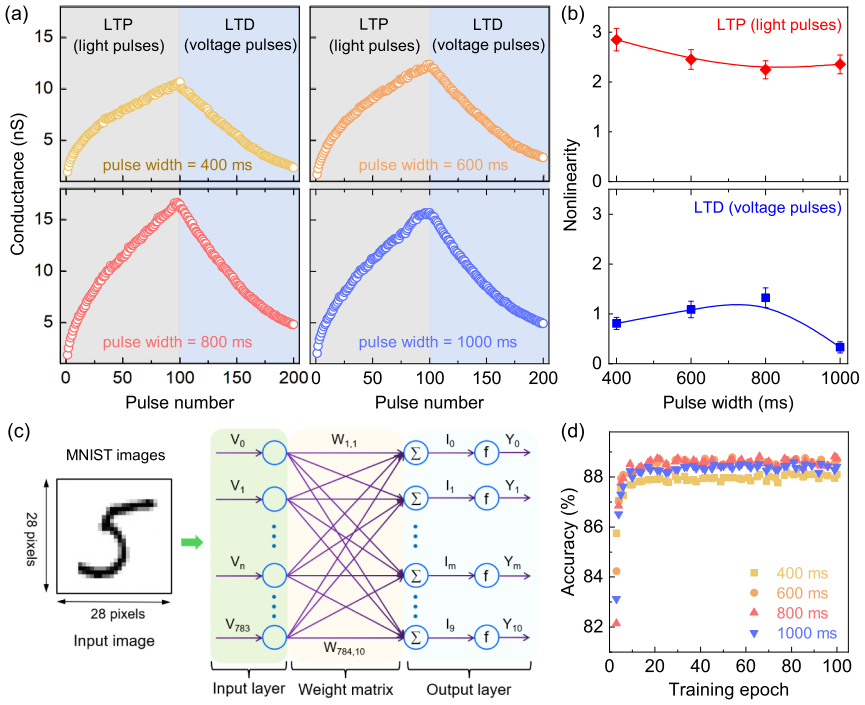

Figure 5. (a) Potentiation and depression emulated by an artificial opto-electronic synaptic transistor under various pulse widths (400, 600, 800, and 1000 ms) with 100 consecutive pulses. LTP is obtained by light pulses (405 nm, pulse period is 1.6 s, and laser power density is 43.3 mW/cm^2). LTD is measured by adjusting the amplitude of voltage pulses from 0.15 to 15 V with a step of 0.15 V. (b) NL of LTP (upper panel) and LTD (lower panel) as a function of pulse width. (c) Schematic of an ANN structure which is simulated with the standard back-propagation algorithm. (d) Recognition accuracy evolution as a function of training epochs for 28 × 28 pixel hand-written MNIST digit images based on the LTP and LTD characteristic curves measured under light and voltage pulse spikes, respectively.

the dark current before stimulation, and "1" denotes the maximum photocurrent soon after pulsed light stimulations. The current of all four pixels is quite low in the dark before stimuli. Figure 4b reveals an STM characteristic since the pixels return to the original state after 10 min. In the case of Pattern #2 (cf. Figure 4c), after the 1 Hz pulsed light stimuli, the irradiated and unirradiated pixels are well recognized due to the relatively high current contrast. LTM behavior has been achieved since the higher frequency (1 Hz) spikes result in a longer pattern retention compared to that stimulated by lower frequency (0.2 Hz) spikes (Pattern #1). This phenomenon was also obtained in other artificial synapses based on layered black phosphorus, which is not stable under an air condition.[8] After the LTM simulation, a voltage pulse (+80 V, 5 s) is applied to perform a reset of the pixel information. The integration of optically written and electrically erased artificial synaptic arrays further highlights the flexibility for artificial vision systems.

3.3. Artificial Neural Network for Pattern Recognition. The LTP and LTD demonstrate a continuous increase and decrease in the PSC under consecutive stimulations at a synapse, respectively. The LTP/LTD characteristic curves of HfS_2-based synapses for different light pulse widths have been investigated, as illustrated in Figure 5a. The LTP was measured under 100 sequential light pulses with pulse widths of 400, 600, 800, and 1000 ms at a fixed power density of 43.3 mW/cm^2. The LTD was modulated by 100 voltage pulses with gradually increasing amplitude from 0.15 to 15 V at a step of 0.15 V. Under continuous light stimulation, the conductance of the channel gradually increases with increasing number of light pulses. On the other hand, it gradually decreases as the pulse number increases under consecutive positive gate voltage pulses. The LTP/LTD profiles for different pulse widths reveal that a wider light pulse will induce a high conductance (cf. Figure S6). In order to further investigate the weight update rule in the ANN simulations used for recognition of hand-written number and digital images, the nonlinearity (NL) is calculated by fitting LTP/LTD profiles with the following equations[46]

$$G_{n+1} = G_n + \alpha_p e^{-\beta_p \frac{G_n - G_{min}}{G_{max} - G_{min}}} \quad (1)$$

$$G_{n+1} = G_n - \alpha_d e^{-\beta_d \frac{G_{max} - G_n}{G_{max} - G_{min}}} \quad (2)$$

where G_n and G_{n+1} are the conductance of the nth and $(n+1)$th pulses, G_{min} and G_{max} are the minimum and maximum conductance, α_p and α_d denote the step size of the conductance between two points in the potentiation and depression curves, and β_p and β_d are the NL of the potentiation and depression curves, respectively. Figure 5b shows the NL as a function of pulse width. It is found that the NL values (~1) derived from the LTD curves are smaller than those (~2.5) obtained from the LTP curves. The NL values of the LTP characteristic curves decreased from 2.85 to 2.24 first and then increased to 2.35 as the light pulse width increased from 0.4 to 1 s because more electron−hole pairs can be generated by a light pulse with a larger width. Furthermore, the relation between laser power and plasticity has been investigated, as shown in Figure S8 (Supporting Information). As the light power intensity increases from 7.7 to 35.7 mW/cm^2, the NL values show an increasing trend from 1.6 to 3.2. It suggests that the width and power of a light pulse have a significant effect on the performance of the ANN.

In order to demonstrate the application of our devices to the neuromorphic calculation of artificial vision systems, Figure 5c

https://doi.org/10.1021/acsami.1c14332
ACS Appl. Mater. Interfaces 2021, 13, 50132−50140

illustrates an example of machine learning by simulating an ANN based on the measured long-term plasticity characteristics (LTP and LTD). First, we classify 28 × 28 pixel handwritten digit images adopted from the MNIST data set by designing a single-layer perceptron model with a back-propagation algorithm.[47] The network is composed of 784 input neurons (V_0−V_{783}), 150 hidden neurons, and 10 output neurons. The input image with 28 × 28 pixels and the obtained digits (Y_0−Y_9) serve as the input and output vectors, respectively. In the simulation process, each neuron receives the value corresponding to the image pixel in the input layer, assigns it to the input vector (V_m), and then converts it into 10 output values to supply the output neuron through the weight matrix ($W_{m,n}$). Here, the synapse weight is expressed as the difference between the conductance values of two equivalent synaptic devices.[48] Note that the conductance of synaptic devices implemented in hardware is always positive, whereas it has positive and negative values in software. In particular, the ANN is trained with one-way and two-way update methods, and the MNIST recognition rates of these cases were compared. With the method, 60 000 images from the MNIST data set are used to train the ANN at each training epoch. The training epoch-dependent recognition accuracies of LTP/LTD curves with different pulse widths (400, 600, 800, and 1000 ms) of HfS_2-based synapses are shown in Figure 5d. It suggests that the recognition accuracy value of the opto-electronic neural network can be as high as 88.5%. Moreover, the relevant curves trained with the two-way update method have been plotted in Figure S9 (Supporting Information).

4. CONCLUSIONS

In summary, the 2D layered HfS_2 semiconductor with excellent photo-electric response is utilized to construct synapses for neuromorphic vision sensors. It is demonstrated that the *n*-type HfS_2-based synaptic devices can simulate the synaptic plasticity of biological synapses under various pulsed light conditions. As the optic spike rate (frequency) increases, the STM can be transformed into LTM, corresponding to the learning, remembering, and forgetting behavior of the human brain. In a further step, the synaptic devices are integrated into 2 × 2 array pixel images to mimic human-like brain behaviors. Finally, the LTP/LTD was realized through the combination of pulsed light and electrical stimulations. Moreover, an ANN for MNIST hand-written number recognition is constructed with a recognition accuracy of about 88.5%. The synaptic plasticity behaviors of HfS_2-based synaptic devices and the high recognition rate provide a new option for developing an efficient artificial vision system.

■ ASSOCIATED CONTENT

Supporting Information

The Supporting Information is available free of charge at https://pubs.acs.org/doi/10.1021/acsami.1c14332.

Top-view of a synaptic opto-electronic device photographed by an optical microscope and Raman spectra of a HfS_2 single crystal and the as-transferred sheet; transfer characteristic curves of the layered HfS_2-based transistors; statistical distribution of the transfer characteristic curves, on/off ratio, mobility, and threshold voltages of 20 devices; PSC behavior of a HfS_2-based synapse transistor stimulated by pulsed light; PSC of a synaptic transistor by applying different amplitudes of pulsed gate voltage; long-term synaptic plasticity characteristics of the four synaptic transistors under different pulse widths; potentiation and depression emulated by an artificial opto-electronic synaptic transistor under various light power densities with 100 consecutive pulses; and evolution of the recognition accuracy of 28 × 28 pixel handwritten MNIST digital images as a function of the training epoch measured under the characteristic curves of light pulses and voltage pulses (PDF)

■ AUTHOR INFORMATION

Corresponding Authors

Jinzhong Zhang − *Technical Center for Multifunctional Magneto-Optical Spectroscopy (Shanghai), Engineering Research Center of Nanophotonics & Advanced Instrument (Ministry of Education), Department of Materials, School of Physics and Electronic Science, East China Normal University, Shanghai 200241, China; Chongqing Key Laboratory of Precision Optics, Chongqing Institute of East China Normal University, Chongqing 401123, China;* orcid.org/0000-0003-1511-4281; Phone: +86-21-54345150; Email: jzzhang@ee.ecnu.edu.cn; Fax: +86-21-54342933

Zhigao Hu − *Technical Center for Multifunctional Magneto-Optical Spectroscopy (Shanghai), Engineering Research Center of Nanophotonics & Advanced Instrument (Ministry of Education), Department of Materials, School of Physics and Electronic Science, East China Normal University, Shanghai 200241, China; Collaborative Innovation Center of Extreme Optics, Shanxi University, Taiyuan, Shanxi 030006, China; Shanghai Institute of Intelligent Electronics & Systems, Fudan University, Shanghai 200433, China;* orcid.org/0000-0003-0575-2191; Phone: +86-21-54345150; Email: zghu@ee.ecnu.edu.cn; Fax: +86-21-54342933

Authors

Hao Xiong − *Technical Center for Multifunctional Magneto-Optical Spectroscopy (Shanghai), Engineering Research Center of Nanophotonics & Advanced Instrument (Ministry of Education), Department of Materials, School of Physics and Electronic Science, East China Normal University, Shanghai 200241, China*

Liping Xu − *Technical Center for Multifunctional Magneto-Optical Spectroscopy (Shanghai), Engineering Research Center of Nanophotonics & Advanced Instrument (Ministry of Education), Department of Materials, School of Physics and Electronic Science, East China Normal University, Shanghai 200241, China; Center for Advanced Electronic Materials and Devices, School of Electronic Information and Electrical Engineering, Shanghai Jiao Tong University, Shanghai 200240, China*

Caifang Gao − *Technical Center for Multifunctional Magneto-Optical Spectroscopy (Shanghai), Engineering Research Center of Nanophotonics & Advanced Instrument (Ministry of Education), Department of Materials, School of Physics and Electronic Science, East China Normal University, Shanghai 200241, China*

Qing Zhang − *Technical Center for Multifunctional Magneto-Optical Spectroscopy (Shanghai), Engineering Research Center of Nanophotonics & Advanced Instrument (Ministry of Education), Department of Materials, School of Physics*

and Electronic Science, East China Normal University, Shanghai 200241, China

Menghan Deng − *Technical Center for Multifunctional Magneto-Optical Spectroscopy (Shanghai), Engineering Research Center of Nanophotonics & Advanced Instrument (Ministry of Education), Department of Materials, School of Physics and Electronic Science, East China Normal University, Shanghai 200241, China*

Qiangfei Wang − *Technical Center for Multifunctional Magneto-Optical Spectroscopy (Shanghai), Engineering Research Center of Nanophotonics & Advanced Instrument (Ministry of Education), Department of Materials, School of Physics and Electronic Science, East China Normal University, Shanghai 200241, China*

Dirk Fuchs − *Institute for Quantum Materials and Technologies, Karlsruhe Institute of Technology, Karlsruhe 75021, Germany*

Wenwu Li − *Technical Center for Multifunctional Magneto-Optical Spectroscopy (Shanghai), Engineering Research Center of Nanophotonics & Advanced Instrument (Ministry of Education), Department of Materials, School of Physics and Electronic Science, East China Normal University, Shanghai 200241, China;* orcid.org/0000-0002-9307-1566

Anyang Cui − *Technical Center for Multifunctional Magneto-Optical Spectroscopy (Shanghai), Engineering Research Center of Nanophotonics & Advanced Instrument (Ministry of Education), Department of Materials, School of Physics and Electronic Science, East China Normal University, Shanghai 200241, China*

Liyan Shang − *Technical Center for Multifunctional Magneto-Optical Spectroscopy (Shanghai), Engineering Research Center of Nanophotonics & Advanced Instrument (Ministry of Education), Department of Materials, School of Physics and Electronic Science, East China Normal University, Shanghai 200241, China;* orcid.org/0000-0003-2341-3978

Kai Jiang − *Technical Center for Multifunctional Magneto-Optical Spectroscopy (Shanghai), Engineering Research Center of Nanophotonics & Advanced Instrument (Ministry of Education), Department of Materials, School of Physics and Electronic Science, East China Normal University, Shanghai 200241, China*

Junhao Chu − *Technical Center for Multifunctional Magneto-Optical Spectroscopy (Shanghai), Engineering Research Center of Nanophotonics & Advanced Instrument (Ministry of Education), Department of Materials, School of Physics and Electronic Science, East China Normal University, Shanghai 200241, China; Collaborative Innovation Center of Extreme Optics, Shanxi University, Taiyuan, Shanxi 030006, China; Shanghai Institute of Intelligent Electronics & Systems, Fudan University, Shanghai 200433, China*

Complete contact information is available at: https://pubs.acs.org/10.1021/acsami.1c14332

Author Contributions

H.X. and L.X. contributed equally. H.X., Q.Z., and Q.W. fabricated the devices. M.D., H.X., and A.C. performed the structural analysis. H.X., L.X., and C.G. performed the electronic and photo-electric measurements. H.X., D.F., and L.X. wrote the manuscript. J.Z., Z.H., and J.C. supervised the research. W.L., K.J., and L.S. contributed to the discussions. All authors have given approval to the final version of the manuscript.

Notes

The authors declare no competing financial interest.

■ ACKNOWLEDGMENTS

The authors thank Z. Fu and L. He for the neural network simulations. This work was financially supported by the National Natural Science Foundation of China (grant nos. 62074058, 91833303, 61805081, 61974043, 62090013, and 61774061), the National Key R&D Program of China (grant no. 2019YFB2203403), the Projects of Science and Technology Commission of Shanghai Municipality (grant nos. 18JC1412400, 19ZR1473400, 18YF1407000, and 19511120100), China Postdoctoral Science Foundation (grant nos. 2020TQ0099 and 2020M681222), the Program for Professor of Special Appointment (Eastern Scholar) at Shanghai Institutions of Higher Learning, the Shanghai Pujiang Program (20PJ1403600), and the Fundamental Research Funds for the Central Universities.

■ REFERENCES

(1) Hines, P. J. Development of Human Brain Neurons. *Science* **2018**, *362*, 788−790.

(2) Todo, Y.; Tang, Z.; Todo, H.; Ji, J.; Yamashita, K. Neurons with Multiplicative Interactions of Nonlinear Synapses. *Int. J. Neural Syst.* **2019**, *29*, 1950012.

(3) Kawato, M.; Furukawa, K.; Suzuki, R. A Hierarchical Neural-Network Model for Control and Learning of Voluntary Movement. *Biol. Cybern.* **1987**, *57*, 169−185.

(4) Mead, C. Neuromorphic Electronic Systems. *Proc. IEEE* **1990**, *78*, 1629−1636.

(5) Merolla, P. A.; Arthur, J. V.; Alvarez-Icaza, R.; Cassidy, A. S.; Sawada, J.; Akopyan, F.; Jackson, B. L.; Imam, N.; Guo, C.; Nakamura, Y.; Brezzo, B.; Vo, I.; Esser, S. K.; Appuswamy, R.; Taba, B.; Amir, A.; Flickner, M. D.; Risk, W. P.; Manohar, R.; Modha, D. S. A Million Spiking-Neuron Integrated Circuit with a Scalable Communication Network and Interface. *Science* **2014**, *345*, 668−673.

(6) Yang, X.; Xiong, Z.; Chen, Y.; Ren, Y.; Zhou, L.; Li, H.; Zhou, Y.; Pan, F.; Han, S.-T. A Self-Powered Artificial Retina Perception System for Image Preprocessing Based on Photovoltaic Devices and Memristive Arrays. *Nano Energy* **2020**, *78*, 105246.

(7) Seo, S.; Jo, S.-H.; Kim, S.; Shim, J.; Oh, S.; Kim, J.-H.; Heo, K.; Choi, J.-W.; Choi, C.; Oh, S.; Kuzum, D.; Wong, H.-S. P.; Park, J.-H. Artificial Optic-Neural Synapse for Colored and Color-Mixed Pattern Recognition. *Nat. Commun.* **2018**, *9*, 5106.

(8) Ahmed, T.; Tahir, M.; Low, M. X.; Ren, Y.; Tawfik, S. A.; Mayes, E. L. H.; Kuriakose, S.; Nawaz, S.; Spencer, M. J. S.; Chen, H.; Bhaskaran, M.; Sriram, S.; Walia, S. Fully Light-Controlled Memory and Neuromorphic Computation in Layered Black Phosphorus. *Adv. Mater.* **2021**, *33*, 2004207.

(9) Yu, J.; Yang, X.; Gao, G.; Xiong, Y.; Wang, Y.; Han, J.; Chen, Y.; Zhang, H.; Sun, Q.; Wang, Z. L. Bioinspired Mechano-Photonic Artificial Synapse Based on Graphene/MoS_2 Heterostructure. *Sci. Adv.* **2021**, *7*, No. eabd9117.

(10) Abbott, L. F.; Regehr, W. G. Synaptic Computation. *Nature* **2004**, *431*, 796−803.

(11) Ahmed, T.; Kuriakose, S.; Mayes, E. L. H.; Ramanathan, R.; Bansal, V.; Bhaskaran, M.; Sriram, S.; Walia, S. Optically Stimulated Artificial Synapse Based on Layered Black Phosphorus. *Small* **2019**, *15*, 1900966.

(12) Zhou, F.; Zhou, Z.; Chen, J.; Choy, T. H.; Wang, J.; Zhang, N.; Lin, Z.; Yu, S.; Kang, J.; Wong, H.-S. P.; Chai, Y. Optoelectronic Resistive Random Access Memory for Neuromorphic Vision Sensors. *Nat. Nanotechnol.* **2019**, *14*, 776−782.

(13) Huber, D.; Petreanu, L.; Ghitani, N.; Ranade, S.; Hromádka, T.; Mainen, Z.; Svoboda, K. Sparse optical microstimulation in barrel cortex drives learned behaviour in freely moving mice. *Nature* **2008**, *451*, 61−64.
(14) Pastrana, E. Optogenetics: Controlling Cell Function with Light. *Nat. Methods* **2011**, *8*, 24−25.
(15) Wang, Y.; Yin, L.; Huang, W.; Li, Y.; Huang, S.; Zhu, Y.; Yang, D.; Pi, X. Optoelectronic Synaptic Devices for Neuromorphic Computing. *Adv. Intell. Syst.* **2021**, *3*, 2000099.
(16) Li, H.; Li, C.; Tao, B.; Gu, S.; Xie, Y.; Wu, H.; Zhang, G.; Wang, G.; Zhang, W.; Chang, H. Two-Dimensional Metal Telluride Atomic Crystals: Preparation, Physical Properties, and Applications. *Adv. Funct. Mater.* **2021**, *31*, 2010901.
(17) Liu, Y.; Duan, X.; Shin, H.-J.; Park, S. J.; Huang, Y.; Duan, X. F. Promises and Prospects of Two-Dimensional Transistors. *Nature* **2021**, *591*, 43−53.
(18) Liang, Q.; Zhang, Q.; Zhao, X.; Liu, M.; Wee, A. T. S. Defect Engineering of Two-Dimensional Transition-Metal Dichalcogenides: Applications, Challenges, and Opportunities. *ACS Nano* **2021**, *15*, 2165−2181.
(19) Jiang, T.; Yin, K.; Wang, C.; You, J.; Ouyang, H.; Miao, R.; Zhang, C.; Wei, K.; Li, H.; Chen, H.; Zhang, R.; Zheng, X.; Xu, Z.; Cheng, X.; Zhang, H. Ultrafast Fiber Lasers Mode-Locked by Two-Dimensional Materials: Review and Prospect. *Photonics Res.* **2019**, *8*, 78.
(20) Jeon, H.; Kim, S. G.; Park, J.; Kim, S. H.; Park, E.; Kim, J.; Yu, H. Y. Hysteresis Modulation on Van der Waals-Based Ferroelectric Field-Effect Transistor by Interfacial Passivation Technique and Its Application in Optic Neural Networks. *Small* **2020**, *16*, 2004371.
(21) Luo, Z.-D.; Xia, X.; Yang, M.-M.; Wilson, N. R.; Gruverman, A.; Alexe, M. Artificial Optoelectronic Synapses Based on Ferroelectric Field-Effect Enabled 2D Transition Metal Dichalcogenide Memristive Transistors. *ACS Nano* **2020**, *14*, 746−754.
(22) Tang, J.; He, C.; Tang, J.; Yue, K.; Zhang, Q.; Liu, Y.; Wang, Q.; Wang, S.; Li, N.; Shen, C.; Zhao, Y.; Liu, J.; Yuan, J.; Wei, Z.; Li, J.; Watanabe, K.; Taniguchi, T.; Shang, D.; Wang, S.; Yang, W.; Yang, R.; Shi, D.; Zhang, G. A Reliable All 2D Materials Artificial Synapse for High Energy-Efficient Neuromorphic Computing. *Adv. Funct. Mater.* **2021**, *31*, 2011083.
(23) Huh, W.; Lee, D.; Lee, C. H. Memristors Based on 2D Materials as an Artificial Synapse for Neuromorphic Electronics. *Adv. Mater.* **2020**, *32*, 2002092.
(24) Gao, C.; Lee, M. P.; Li, M.; Lee, K. C.; Yang, F. S.; Lin, C. Y.; Watanabe, K.; Taniguchi, T.; Chiu, P. W.; Lien, C. H.; Wu, W. W.; Lin, S. P.; Li, W.; Lin, Y. F.; Chu, J. Mimic Drug Dosage Modulation for Neuroplasticity Based on Charge-Trap Layered Electronics. *Adv. Funct. Mater.* **2020**, *31*, 2005182.
(25) Ulaganathan, R. K.; Sankar, R.; Lin, C. Y.; Murugesan, R. C.; Tang, K.; Chou, F. C. High-Performance Flexible Broadband Photodetectors Based on 2D Hafnium Selenosulfide Nanosheets. *Adv. Electron. Mater.* **2020**, *6*, 1900794.
(26) Xu, K.; Wang, Z.; Wang, F.; Huang, Y.; Wang, F.; Yin, L.; Jiang, C.; He, J. Ultrasensitive Phototransistors Based on Few-Layered HfS_2. *Adv. Mater.* **2015**, *27*, 7881−7887.
(27) Xu, K.; Huang, Y.; Chen, B.; Xia, Y.; Lei, W.; Wang, Z.; Wang, Q.; Wang, F.; Yin, L.; He, J. Toward high-performance top-gate ultrathin HfS_2 field-effect transistors by interface engineering. *Small* **2016**, *12*, 3106−3111.
(28) Paszke, A.; Gross, S.; Massa, F.; Lerer, A.; Bradbury, J.; Chanan, G.; Killeen, T.; Lin, Z.; Gimelshein, N.; Antiga, L.; Desmaison, A.; Kopf, A.; Yang, E.; DeVito, Z.; Raison, M.; Tejani, A.; Chilamkurthy, S.; Steiner, B.; Fang, L.; Bai, J.; Chintala, S. *Advances in Neural Information Processing Systems 32*; Curran Associates, Inc., 2019, pp 8024−8035.
(29) Sangwan, V. K.; Hersam, M. C. Neuromorphic Nanoelectronic Materials. *Nat. Nanotechnol.* **2020**, *15*, 517−528.
(30) Roubi, L.; Carlone, C. Resonance Raman Spectrum of HfS_2 and ZrS_2. *Phys. Rev. B* **1988**, *37*, 6808−6812.
(31) Guo, Y.; Wei, X.; Shu, J.; Liu, B.; Yin, J.; Guan, C.; Han, Y.; Gao, S.; Chen, Q. Charge Trapping At The MoS_2-SiO_2 Interface and Its Effects on the Characteristics of MoS_2 Metal-Oxide-Semiconductor Field Effect Transistors. *Appl. Phys. Lett.* **2015**, *106*, 103109.
(32) Nasr, J. R.; Schulman, D. S.; Sebastian, A.; Horn, M. W.; Das, S. Mobility Deception in Nanoscale Transistors: An Untold Contact Story. *Adv. Mater.* **2019**, *31*, 1806020.
(33) Prasad, S.; Galetta, S. L. Anatomy and Physiology of the Afferent Visual System. *Handb. Clin. Neurol.* **2011**, *102*, 3−19.
(34) Martin, S. J.; Grimwood, P. D.; Morris, R. G. M. Synaptic Plasticity and Memory: An Evaluation of the Hypothesis. *Annu. Rev. Neurosci.* **2000**, *23*, 649−711.
(35) Zhang, C.; Gong, C.; Nie, Y.; Min, K.-A.; Liang, C.; Oh, Y. J.; Zhang, H.; Wang, W.; Hong, S.; Colombo, L.; Wallace, R. M.; Cho, K. Systematic study of electronic structure and band alignment of monolayer transition metal dichalcogenides in Van der Waals heterostructures. *2D Mater.* **2016**, *4*, 015026.
(36) Brzosko, Z.; Mierau, S. B.; Paulsen, O. Neuromodulation of Spike-Timing-Dependent Plasticity: Past, Present, and Future. *Neuron* **2019**, *103*, 563−581.
(37) Yang, C. S.; Shang, D. S.; Liu, N.; Fuller, E. J.; Agrawal, S.; Talin, A. A.; Li, Y. Q.; Shen, B. G.; Sun, Y. All-Solid-State Synaptic Transistor with Ultralow Conductance for Neuromorphic Computing. *Adv. Funct. Mater.* **2018**, *28*, 1804170.
(38) Chang, T.; Jo, S.-H.; Lu, W. Short-Term Memory to Long-Term Memory Transition in a Nanoscale Memristor. *ACS Nano* **2011**, *5*, 7669−7676.
(39) Malenka, R. C.; Bear, M. F. LTP and LTD: an Embarrassment of Riches. *Neuron* **2004**, *44*, 5−21.
(40) Wang, Y.; Lv, Z.; Chen, J.; Wang, Z.; Zhou, Y.; Zhou, L.; Chen, X.; Han, S.-T. Photonic Synapses Based on Inorganic Perovskite Quantum Dots for Neuromorphic Computing. *Adv. Mater.* **2018**, *30*, 1802883.
(41) Lee, K.-C.; Li, M.; Chang, Y.-H.; Yang, S.-H.; Lin, C.-Y.; Chang, Y.-M.; Yang, F.-S.; Watanabe, K.; Taniguchi, T.; Ho, C.-H.; Lien, C.-H.; Lin, S.-P.; Chiu, P.-W.; Lin, Y.-F. Inverse Paired-Pulse Facilitation in Neuroplasticity Based on Interface-Boosted Charge Trapping Layered Electronics. *Nano Energy* **2020**, *77*, 105258.
(42) Zucker, R. S.; Regehr, W. G. Short-Term Synaptic Plasticity. *Annu. Rev. Physiol.* **2002**, *64*, 355−405.
(43) Rubin, D. C.; Wenzel, A. E. One Hundred Years of Forgetting: A Quantitative Description of Retention. *Physiol. Rev.* **1996**, *103*, 734−760.
(44) Gerstner, W.; Kistler, W. M. *Spiking Neuron Models: Single Neurons, Populations, Plasticity*; Cambridge University Press: Cambridge, U.K., New York, 2002.
(45) Xu, C.; Zhao, M.-X.; Poo, M.-M.; Zhang, X.-H. GABAB Receptor Activation Mediates Frequency-Dependent Plasticity of Developing Gabaergic Synapses. *Nat. Neurosci.* **2008**, *11*, 1410−1418.
(46) Sun, J.; Oh, S.; Choi, Y.; Seo, S.; Oh, M. J.; Lee, M.; Lee, W. B.; Yoo, P. J.; Cho, J. H.; Park, J.-H. Optoelectronic Synapse Based on IGZO-Alkylated Graphene Oxide Hybrid Structure. *Adv. Funct. Mater.* **2018**, *28*, 1804397.
(47) Lecun, Y.; Bottou, L.; Bengio, Y.; Haffner, P. Gradient-Based Learning Applied to Document Recognition. *Proc. IEEE* **1998**, *86*, 2278−2324.
(48) Qian, C.; Oh, S.; Choi, Y.; Kim, J.-H.; Sun, J.; Huang, H.; Yang, J.; Gao, Y.; Park, J.-H.; Cho, J. H. Solar-Stimulated Optoelectronic Synapse Based on Organic Heterojunction with Linearly Potentiated Synaptic Weight for Neuromorphic Computing. *Nano Energy* **2019**, *66*, 104095.

https://doi.org/10.1021/acsami.1c14332
ACS Appl. Mater. Interfaces 2021, 13, 50132−50140